



Confocal Raman spectromicroscopy for tin-core/carbon-shell nanowire heterostructure

Fengping Wang^{a,*}, Ruying Li^b, Xueliang Sun^{b,*}, Zhifeng Ding^{c,*}

^a Department of Physics, University of Science and Technology Beijing, Beijing 100083, China

^b Department of Mechanical and Materials Engineering, University of Western Ontario, London, Ontario, Canada N6A 5B9

^c Department of Chemistry, University of Western Ontario, London, Ontario, Canada N6A 3K7

ARTICLE INFO

Article history:

Received 24 February 2011

Received in revised form 2 September 2011

Accepted 2 September 2011

Available online 10 September 2011

Keywords:

Nanoheterostructure

Raman spectromicroscopy

Nano-crystalline graphite

Luminescence

ABSTRACT

High density heterostructures of carbon nanotubes encapsulated single crystalline tin nanowires have been characterized by Raman spectromicroscopy. The morphology, composition and structure of the synthesized nanoheterostructures were examined by using scanning electron microscopy, transmission electron microscopy. The Raman spectra obviously manifest the crystalline nano-graphite within amorphous carbon walls in the heterostructures. The Raman image reproduces the pristine heterostructures of the CNTs as seen in SEM image, which illustrate the single nanowires oriented uniformly grown on micro-graphitic fibers. It was found that the resultant heterostructures are luminescent which was attributed to crystalline nano-graphite embedded in the amorphous carbon matrix, which is a consequence of excitons localization within an increasing number of sp^2 rich clusters. The contrast in the Raman image reflects nonuniform distribution of the graphite cluster size which acts as the radiative centers. The luminescent property was reviewed. The enhanced Raman spectra and luminescent property by the well-defined tin nanowires inside the heterostructures was revealed.

© 2011 Elsevier B.V. All rights reserved.

1. Introduction

Over last decades, carbon allotrope, because of its catenation properties, as well as a simple variation in its local bonding configuration giving rise to a variety of materials as diverse as diamond, graphite, fullerenes, and disordered, amorphous and nanostructured carbons including nanocrystalline diamond and carbon nanotubes (CNTs), have attracted significant research efforts [1]. Especially CNTs, because of their excellent physical and chemical properties as well as tremendous potential for applications in composite materials, electrode materials, field emitters, nanoelectronics and nanosensors [2], have greatly attracted both academic and industrial attention. Further, considerable effort has been made to explore various heterostructures with the combination of CNTs and nanowires. Such one-dimensional (1D) heterostructures are of significance to both fundamental studies in nanoscience and potential industrial applications in nanotechnology. The challenge for the applications of the carbon allotrope and related heterostructures is to achieve perfect control of nanoscale-related properties. This obviously requires correlating the physical and chemical properties with the resulting nanostructure. Confocal

Raman spectromicroscopy (CRSM) has already proven to be a general characterization method for characterization of crystallinity, morphology and chemical structures. Not only can it provide basic phase identification but also subtle spectra alterations can be used to assess nanoscale structural changes and characterize micromechanical behaviour [3]. CRSM is thus a unique tool for probing or mapping nanophases dispersed in a matrix. Raman spectroscopy (RS) has historically played an important role in the structural characterization of graphitic materials, in particular providing valuable information about defects, disorder in graphite-based systems stacking of the graphene layers and the finite sizes of the crystallites parallel and perpendicular to the hexagonal axis. It has been widely used in the last four decades to characterize graphitic systems, such as pyrolytic graphite, carbon fibers, glassy carbon, nanographite ribbons, fullerenes, carbon nanotubes and heterogeneous carbonaceous materials (CM) [4–8]. Micro-Raman spectroscopy is sometimes more powerful than X-ray analysis for detecting and monitoring crystallization/amorphization processes in covalent materials [3]. RS is complementary to HRTEM investigations for heterogeneous CM. It provides quantitative information on the structure that can be difficult to obtain by HRTEM [8].

In this paper, we report the spectra and imaging study by CRSM with single wire resolution, for the high-density, aligned heterostructures of tin nanowires encapsulated in amorphous carbon with nano-crystalline graphite (a-CNT-Sn).

* Corresponding authors. Tel.: +86 10 62332587; fax: +86 10 62332587.
E-mail address: fpwang@ustb.edu.cn (F. Wang).

2. Materials and methods

The a-CNT-Sn was synthesized by thermal evaporation method. Pure commercial grade Sn powders (99.8%) were loaded in an alumina boat placed at the middle of a quartz tube in a horizontal tube furnace. A commercially available carbon paper acted as a substrate for the growth of products. The carbon paper substrate consists of small graphitic fibers, 5–10 μm in diameter. The reaction chamber was heated from room temperature to 900 $^{\circ}\text{C}$ (in about 15 min) under an atmosphere of flowing Ar and 2% ethylene (200 sccm). C_2H_2 gas was introduced into the reaction system simultaneously. The details of the preparation have been described elsewhere [9]. The morphologies, structures and chemical composition of the as-prepared heterostructures were examined by SEM (Hitachi S-2600N, equipped with energy dispersive X-ray (EDX) analysis facility), TEM (JEOL 2010 FEG, 200 kV) and high-resolution transmission electron microscopy in a Tecnai G2 F30 TEM. Confocal Raman spectromicroscopy (Alpha SNOM, WITec, Germany) was conducted under ambient conditions. A YAG linearly polarized laser (Verdi 5, Coherent Inc., Santa Barbara, CA) with a 532 nm wavelength was used for Raman excitation. A power of 10 mW of output from the laser was delivered to objective by an about 2 m single mode fiber for the experiments. A 50 \times objective with 0.75 NA (Nikon Canada, Mississauga, ON) was used to focus the laser beam onto the specimen and collect Raman signals. An edge filter (RazorEdge filters from Semrock, NY) with a band-pass $>160\text{ cm}^{-1}$ was used to block the 532 nm excitation laser. A complete Raman spectrum was recorded at each image pixel by an air-cooled (-70°C), back-illuminated CCD camera (Model DV401-BV, ANDOR) behind a grating (300 or 1800 g mm^{-1}) of a

spectrograph (UHTS300, WITec). The details of the Raman experimental can be seen elsewhere [10].

3. Results and discussion

The SEM image shows that a high-density of nanostructures grows radially on the graphitic fibers from the carbon paper substrate (shown in Fig. 1a). The straight and isolated nanostructures, 5–10 μm in length, 200–300 nm in diameter, are aligned perpendicular to the surface of the graphitic fibers (Fig. 1b). Close examination by using transmission electron microscopy (TEM), as shown in Fig. 2a and b reveals that a dark region, 200–500 nm in length, is present on the tips or/and the bottoms of each nanotube heterostructures, separated from the main light region by the light region. Energy dispersive X-ray (EDX) analysis taken from several fragments of Fig. 2b reveals the carbon nanotube encapsulated tin nanowires in the dark regions and hollow carbon nanotubes in the light region [9]. A high resolution TEM lattice image and selected area electron diffraction (SAED) patterns of the a-CNT-Sn het-

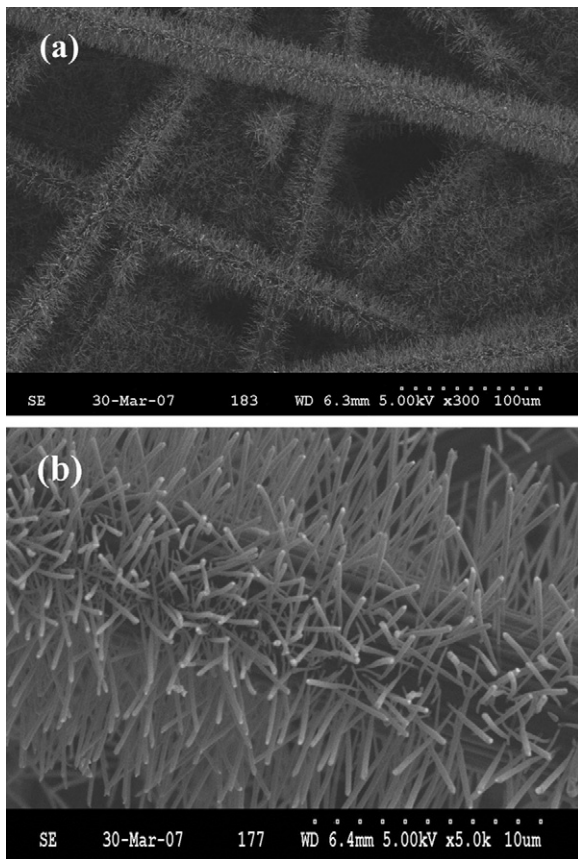


Fig. 1. (a) SEM image showing the morphologies of high-density carbon nanotube encapsulating single crystalline Sn nanowires grown on graphitic fibers, (b) increased magnification SEM images showing the tip of nanostructure array.

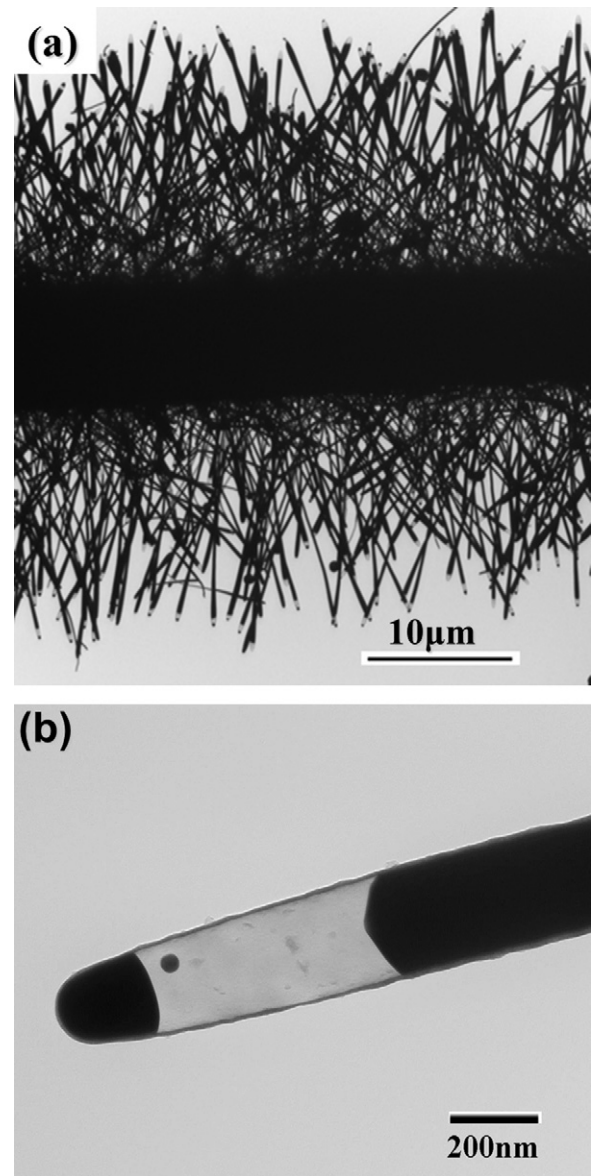


Fig. 2. TEM image of an individual nanostructure showing carbon nanotube encapsulating Sn nanowires, revealing the hollow region located at each tip and bottom region of a heterostructure, respectively.

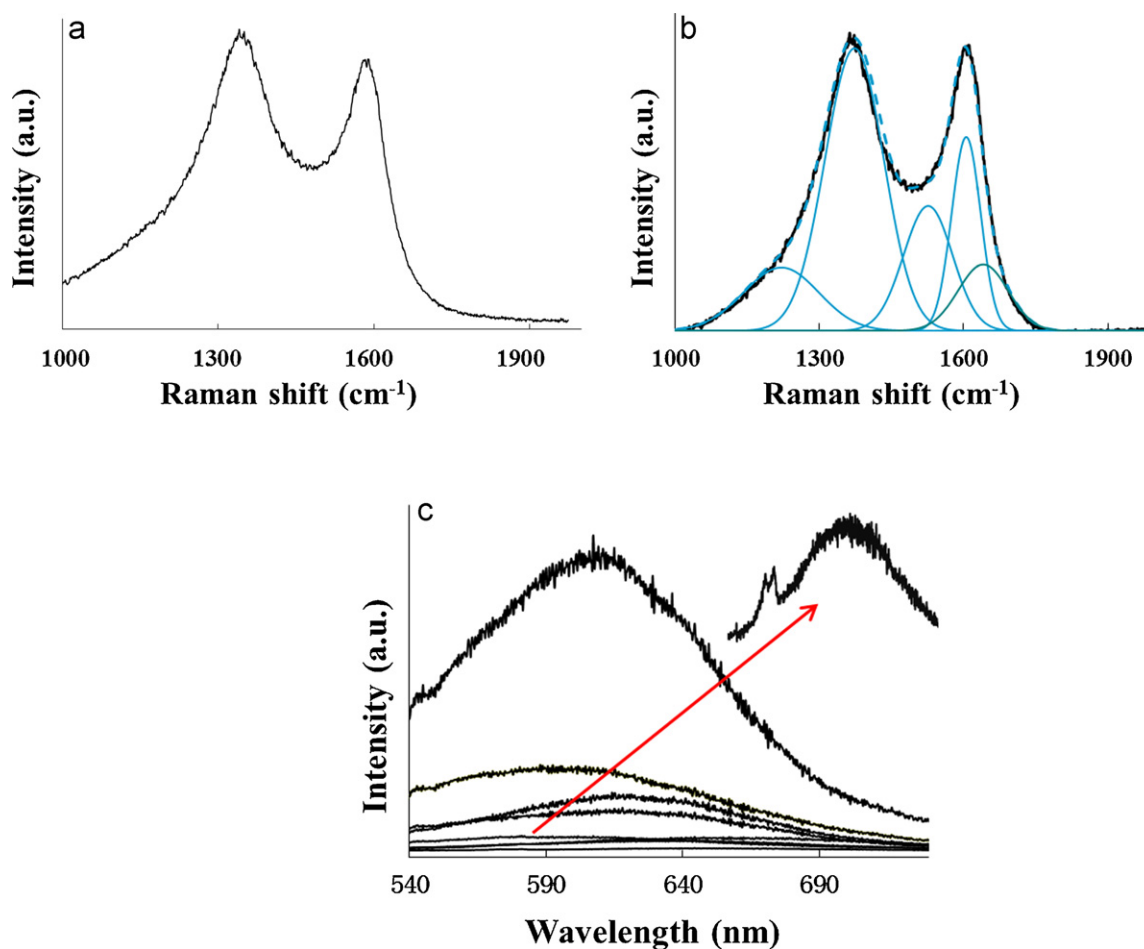


Fig. 3. (a) Raman spectrum for the pristine heterostructures, (b) the fitted Raman spectrum of an examined a-CNT-Sn with PL background subtracted and fitted with Gaussian line shapes to the all constituent peaks, (c) photoluminescent spectrum (the inset in c is the magnification for one luminescent spectrum).

erostuctures confirmed the inside tin nanowires with pure single crystal metallic nature and the carbon encapsulating layer with featureless, suggesting coaxially grown heterostructures, consisting of metallic tin nanowires and an amorphous carbon encapsulating nanotubes. The tin nanowires, 200–400 nm in diameter, are covered with amorphous carbon walls of 30 nm thickness [9].

The Raman spectrum for each sample was measured using 532 nm excitation. Fig. 3a displays a typical Raman spectrum for the as-prepared heterostructures. Prominent D and G bands of the CNTs present clearly at 1350 and 1589 cm⁻¹. It is well known that the G band is a doubly degenerate (*i*TO and LO) phonon mode (E_{2g} symmetry) at the center of Brillouin Zone that is due to the in-plane bond stretching of all pairs of sp^2 bonded C atoms in both rings and chains. The D band usually assigned to K-point phonons of A_{1g} symmetry is attributed to the breathing mode of aromatic rings [5,11–14]. This mode is forbidden in perfect graphite and only becomes active in the presence of disorder, activated by the relaxation of the $q=0$ selection rule. Its intensity is strictly connected to the presence of sixfold aromatic ring. G and D peaks, of varying intensity, position, and width, dominate the Raman spectra of nanocrystalline and amorphous carbons, even those without widespread graphitic ordering [5]. The D-band grows in intensity with increasing disorder or decreasing crystal size. It can be observed from Fig. 3a that, in one hand, the G band appears to be broad compared with crystal graphite indicating a high nonuniformity and disorder properties of the CNT walls [3,15–17]; in another hand, compared with Raman spectrum of amorphous carbon, the upward position and hardness of the G peak indicate the nanocrystalline

graphite character [18–20]. As is well-known, the G mode of a-C is at 1510 cm⁻¹. From a-C to nanocrystalline graphite, the G peak moves from 1510 to 1600 cm⁻¹ [5,18]. It shows in Fig. 3a the G peak at 1589 cm⁻¹ indicating the formation of the sp^2 chains, aromatic rings or clusters and localization in the amorphous carbon matrix.

In addition, note that the D peak has a much greater area than the G peak, also that the D peak is much wider than the G peak in Fig. 3a. As we have known that the D peak arises from aromatic rings. Starting from graphite, at a fixed λ , $I(D)/I(G)$ will increase with increasing disorder [5]. For more disorder, clusters decrease in number and become smaller and more distorted, until they open up. For small diameter (L_a) cluster, the D-mode strength is proportional to the probability of finding a sixfold ring in the cluster, that is, proportional to the cluster area [5]. Thus, the strong and wide D band in Fig. 3a indicated disordered graphite character of the CNTs, accompanied by an increase in ordering due to the formation of clusters of aromatic rings. The Raman spectrum shown in Fig. 3a is similar with that of graphitic a-C observed by J. Roberson [21,22]. These clusters of aromatic rings contained in the a-CNT-Sn did not observed in the high resolution TEM and XRD [9] indicating that the Raman spectroscopy is more sensitive to the graphitic a-C structure than TEM and XRD.

To obtain the detailed positions and intensities for the G, D, and related peaks, we fitted the spectra by using the computer program PEAKFIT 4.12 (Jandel Scientific). Fig. 3b shows the spectra of an examined a-CNT-Sn with PL background subtracted and fitted with Gaussian line shapes to the all constituent peaks. We can see that

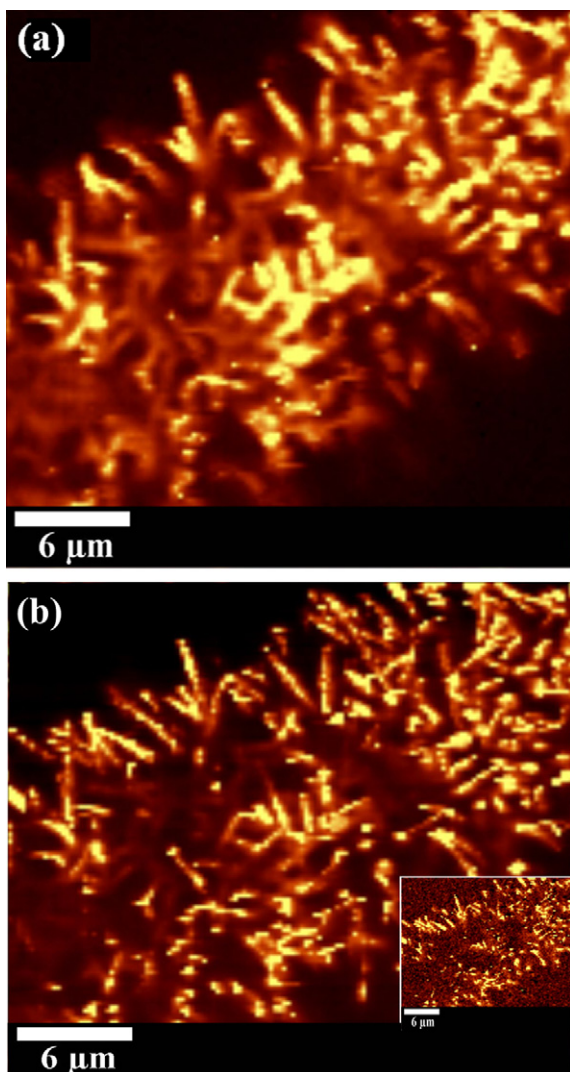


Fig. 4. Raman images (a), the overview image (b), and the luminescent image (the inset b).

besides the D and G band located around 1350 cm^{-1} and 1589 cm^{-1} , additional bands appear in the first-order region around 1181 , 1506 and 1627 cm^{-1} . The 1181 cm^{-1} component appears only in very poorly organized CM, but its attribution is still strongly debated. The 1506 cm^{-1} band, present only as a very wide band in poorly crystallized CM, attributed to defects outside the plane of aromatic layers like tetrahedral carbons [8]. The 1627 cm^{-1} band makes a shoulder on the G band, which is always present when the D band is present and its intensity is usually regarded as a Raman-allowed G-point mode, in fact originates from the same defect-induced, double resonant process as the D mode [23,24].

Interestingly, luminescent character of the heterostructures was observed in the whole observable range. Fig. 3c displays the room temperature photoluminescence (PL) spectrum recorded at identical condition in different regions upon irradiation with a 532 nm laser. The wavelength and intensity of the PL are diverse in different regions, indicating the nonuniform distribution of the size and number of the luminescent centers. The two narrow small peaks located at the range of 570–590 nm in Fig. 3c are the Raman spectra, which are the D and G band, respectively. It also presents the graphitic a-C character. In order to explore and discern the origin of the PL in the a-CNT-Sn, RS and PL image were constructed, respectively. Fig. 4a shows the RS image made by using the D and G

band intensity for each pixel. It clearly reproduces the pristine heterostructures of the CNTs resolution as seen in SEM and TEM image. The Raman image further confirms that the CNTs in heterostructures maintain amorphous carbon with the partial nanocrystalline graphite feature. Fig. 4b shows an overview of a collection of the pristine heterostructures in a $60\text{ }\mu\text{m} \times 60\text{ }\mu\text{m}$ area, which was constructed with the total intensity of the whole spectrum at each pixel (including the Raman and PL intensity). Since the much stronger PL than RS, it can be deduced that the intensity in the image mainly results from the PL. The inset in Fig. 4b is the luminescent image constructed using the PL intensity in the range from the wavenumber larger than 2000 cm^{-1} . Compared with Raman image, it can be observed that the PL image have higher spacial resolution. It could also be seen that the center of the nanowires is much brighter than the fringes, which may remind the enhancement for the PL in the center of the nanowires. The nonuniform contrast in the Raman image reflects nonuniform distribution of the graphite cluster size in the a-CNT. In view of tin nanowires do not give strong luminescence; the strong luminescence of the heterostructures could be derived from the graphitic a-C, which is a consequence of carrier localization within an increasing number of sp^2 rich clusters, similar to those of hydrogen-free a-C [25]. The potentiation of the PL may result from the surface plasmon enhanced PL of tin nanowires. The PL mechanism of the amorphous carbon has been investigated [18–27]. A widely accepted mechanism for the PL in amorphous carbon, is due to the radiative recombination of electrons and holes in the band-tail states created by sp^2 rich clusters from not only carbon NCs of different sizes in the sample but also a distribution of different emissive trap sites. The sp^2 clusters contain different structural units with double conjugated C=C bonds, which act as recombination centers [28]. The resulting PL band is the sum of the luminescence contribution of sp^2 -bonded clusters of various sizes. As a result, the PL peak positions change with various sizes in different region, as seen in Fig. 3c. Such multi-peak position structure can be explained as result of size dependence of the PL spectra. Because of the existence of a size distribution of the clusters, each emitting at its own characteristic energy, the measured PL intensity represents an ensemble average. For excitation at 2.34 eV the larger nanocrystals can be excited into high excited state; nanocrystals of small size can be excited in their lower excited state. As a result PL spectra are excited in different positions. Meanwhile the FWHM of the PL band for lower energy excitation (2.34 eV) becomes broader due to the luminescence from clusters with low photon energy from larger size to high photon energy from small size. To survey overall PL spectra, it have been observed that the increase in the PL intensity correlates well with the increase in D peak, which also suggests that the enhanced PL is a consequence of carrier localization within an increasing number of sp^2 rich clusters. This also prompt further that the carbon outside tin wires in the heterostructures are the amorphous carbon with nano-crystalline graphite property.

4. Conclusions

We have characterized the heterostructures of carbon nanotubes encapsulated single crystalline tin nanowires by employing confocal Raman spectromicroscopy. The spectra show that the nano-crystalline graphite embedded in the a-C walls in the nanowire heterostructures. The fitted spectra further demonstrated that the defects, disordered and aromatic ring clusters carbon contained in the a-CNT-Sn. The SEM image shows that a high-density of nanostructures grows radially on the graphitic fibers. From another perspective, Raman and PL images reproduced this morphology. The resultant heterostructures are luminescent. The luminescent property of the resultant heterostructures could be attributed to nano-crystalline graphite carbon. Carrier localiza-

tion within these clusters is then responsible for the strong PL. The strong PL provides the further verification for the existence of the nano-crystalline graphite in the a-CNT walls.

Acknowledgements

Authors appreciate the financial supports for this research from General Motors of Canada, Natural Science and Engineering Research Council of Canada (NSERC), University of Science and Technology Beijing (fundamental development fund and chancellor Scholarship program) and the University of Western Ontario. Thanks Ms. Jianling Hu for Raman spectrum fitting.

References

- [1] R.H. Baughman, A.A. Zakhidov, A. de Heer, Carbon nanotubes—the route toward applications, *Science* 297 (2002) 787–792.
- [2] J. Hu, Y. Bando, J. Zhan, C. Zhi, D. Golberg, Carbon nanotubes as nanoreactors for fabrication of single-crystalline Mg₃N₂ nanowires, *Nano Lett.* 6 (2006) 1136–1140.
- [3] G. Gouadec, P. Colombari, Raman spectroscopy of nanomaterials: how spectra relate to disorder, particle size and mechanical properties, *Prog. Cryst. Growth CH* 53 (2007) 1–56.
- [4] C. Casiraghi, F. Piazzaa, A.C. Ferrari, D. Grambole, J. Robertson, Bonding in hydrogenated diamond-like carbon by Raman spectroscopy, *Diamond Relat. Mater.* 14 (2005) 1098–1102.
- [5] A.C. Ferrari, J. Robertson, Interpretation of Raman spectra of disordered and amorphous carbon, *Phys. Rev. B* 61 (2000) 14095–14107.
- [6] M. Ramsteiner, J. Wagner, Resonant Raman scattering of hydrogenated amorphous carbon: evidence for π -bonded carbon clusters, *Appl. Phys. Lett.* 51 (1987) 1355–1357.
- [7] A. Pimenta, G. Dresselhaus, M.S. Dresselhaus, L.G. Cancado, A. Jorio, R. Saito, Studying disorder in graphite-based systems by Raman spectroscopy, *Phys. Chem. Chem. Phys.* 9 (2007) 1276–1291.
- [8] O. Beyssac, B. Goffé, J.P. Petit, E. Froigneux, M. Moreau, J.N. Rouzaud, On the characterization of disordered and heterogeneous carbonaceous materials by Raman spectroscopy, *Spectrochim. Acta A* 59 (2003) 2267–2276.
- [9] R. Li, X. Sun, X. Zhou, M. Cai, X. Sun, Aligned heterostructures of single-crystalline tin nanowires encapsulated in amorphous carbon nanotubes, *J. Phys. Chem. C* 111 (2007) 9130–9135.
- [10] F. Wang, X. Zhou, J. Zhou, T.K. Sham, Z. Ding, Observation of single tin dioxide nanoribbons by Raman spectromicroscopy and microspectroscopy, *J. Phys. Chem. C* 111 (2007) 18839–18843.
- [11] R.J. Nemanich, S.A. Solin, First- and second-order Raman scattering from finite-size crystals of graphite, *Phys. Rev. B* 20 (1979) 392–401.
- [12] P. Lespade, R. Al-Jishi, M.S. Dresselhaus, Model for Raman scattering from incompletely graphitized carbons, *Carbon* 20 (1982) 427–431.
- [13] A.C. Ferrari, J. Robertson, Resonant Raman spectroscopy of disordered, amorphous, and diamondlike carbon, *Phys. Rev. B* 64 (2001) 075414–75513.
- [14] K.W.K. Gilkes, H.S. Sands, D.N. Batchelder, J. Robertson, W.I. Milne, Direct observation of sp³ bonding in tetrahedral amorphous carbon using ultraviolet Raman spectroscopy, *Appl. Phys. Lett.* 70 (1997) 1980–1982.
- [15] F. Tuinstra, J.L. Koenig, Raman spectrum of grappite, *J. Chem. Phys.* 53 (1970) 1126–1130.
- [16] S. Reich, C. Thomsen, Raman spectroscopy of grappite, *Phil. Trans. R. Soc. Lond. A* 362 (2004) 2271–2288.
- [17] C.A. Ferrari, Raman spectroscopy of graphene and graphite: disorder, electron–phononcoupling, doping and nonadiabatic effects, *Solid State Commun.* 143 (2007) 47–57.
- [18] M. Rybachuk, J.M. Bell, Electronic states of trans-polyacetylene, poly(p-phenylene vinylene) and sp-hybridised carbon species in amorphous hydrogenated carbon probed by resonant Raman scattering, *Carbon* 47 (2009) 2481–2490.
- [19] E. Barborini, P. Piseri, A. Li Bassi, A.C. Ferrari, C.E. Bottani, P. Milani, Synthesis of carbon films with controlled nanostructure by separation of neutral clusters in supersonic beams, *Chem. Phys. Lett.* 300 (1999) 633–638.
- [20] J. Robertson, Hard amorphous (diamond-like) carbons, *Prog. Solid State Chem.* 21 (1991) 199–333.
- [21] S.J. Henley, J.D. Carey, S.R.P. Silva, Room temperature photoluminescence from nanostructured amorphous carbon, *Appl. Phys. Lett.* 85 (2004) 6236–6238.
- [22] Z.D. Hu, Y.F. Hu, Q. Chen, X.F. Duan, L.-M. Peng, Synthesis and characterizations of amorphous carbon nanotubes by pyrolysis of ferrocene confined within AAM templates, *J. Phys. Chem. B* 110 (2006) 8263–8267.
- [23] S. Reich, C. Thomsen, Raman spectroscopy of graphite, *Phil. Trans. R. Soc. Lond. A* 362 (2004) 2271–2288.
- [24] J. Maultzsch, S. Reich, C. Thomsen, S. Webster, R. Czerw, D.L. Carroll, S.M.C. Vieira, P.R. Birkett, C.A. Rego, Raman characterization of boron-doped multi-walled carbon nanotubes, *Appl. Phys. Lett.* 81 (2002) 2647–2649.
- [25] J. Robertson, Photoluminescence mechanism in amorphous hydrogenated carbon, *Diamond Relat. Mater.* 5 (1996) 457–460.
- [26] Rusli, G.A.J. Amaratunga, S.R.P. Silva, Photoluminescence in amorphous carbon thin films and its relation to the microscopic properties, *Thin Solid Films* 270 (1995) 160–164.
- [27] R. Liu, D. Wu, S. Liu, K. Koyov, W. Knoll, Q. Li, An aqueous route to multicolor photoluminescent carbon dots using silica spheres as carriers, *Angew. Chem. Int. Ed.* 48 (2009) 4598–4601.
- [28] J. Xu, J. Mei, X. Huang, W. Li, Z. Li, X. Li, K. Chen, The change of photoluminescence characteristics of amorphous carbon films due to hydrogen dilution, *J. Non-Crystalline Solids* 338–340 (2004) 481–485.